Continuous Photopolymerization of *n*-Butyl Acrylate Using a Narrow Channel Reactor

R. J. J. Jachuck* and V. Nekkanti

Process Intensification and Clean Technology (PICT), Department of Chemical and Biomolecular Engineering, Clarkson University, Potsdam, New York, USA

Received July 20, 2007; Revised Manuscript Received January 25, 2008

ABSTRACT: This study highlights the potential of using ultraviolet (UV) radiation for initiating polymerization of *n*-butyl acrylate (BA) in a narrow channel reactor made of borosilicate. A continuous flow system using a 90 cm long glass reactor with a circular cross section (1.5 mm internal diameter) was used in conjunction with a UV flood lamp having peak intensity at 365 nm. A series of experiments were performed in order to study the influence of UV intensity, initiator concentration, and space time on conversion and molecular weight distribution. A mathematical model incorporating the reactor geometry has been developed for predicting the conversions, and the results were compared with the experimental findings. Experimental results from this work have been benchmarked against continuous thermal polymerization studies.

1. Introduction

The advantages of photopolymerization have become obvious with increasing demand for solvent-free and energy efficient processing.[1] The use of UV for converting a monomer into polymer has found limited applications in industry. As explained by Jachuck and Dunk,[2] this is due to the inherent design of the conventional chemical reactors which mostly use stirred tanks. Such reactors require considerable penetration depth for the UV radiation and hence make the process energy intensive. It also adversely affects the polymerization process, resulting in polymers with varying degrees of conversion and polydispersity indices. Process intensification promotes the use of films with smaller dimensions to gain better control on the quality of the product. In polymers, polydispersity is used as the measure of the quality. Iwasaki et al.[3] have successfully demonstrated the advantages of process intensification by using microreactors to carry out thermal polymerization. Significant improvement in polydipersity indices has been reported using microreactors as compared to the batch process. Results from photopolymerization experiments are compared to results from Iwasaki et al. to highlight the advantages of the photopolymerization process over thermal based polymerization.

It has been well-known that the use of UV radiation can induce very high rates of initiation that directly affect the overall rate of polymerization.[1,4] So far, work in photopolymerization has been progressed in curing of static films which include dental restorations, optoelectronics, and adhesive applications. Another area this technology is used is in the estimation of kinetic constants in polymerization reactions which include techniques such as pulsed laser polymerization (PLP). Poly(*n*-butyl acrylate) has several uses in the area of coatings and inks, adhesives, sealants, textiles, elastomers, etc.

Photopolymerization using thin static films ranging from 5 to 1000 μm was investigated by various authors.[4,5] It was reported that the extent of nonuniformity in the polymerization kinetics in a film increases with the thickness. Decker et al. have investigated the influence of temperature on photopolymerization kinetics and have found the rates of polymerization to be very high which is attributed to the high rates of initiation and reaction exotherm.[4] Although the results were promising, it is not possible to take advantage of the high reaction rates and use thin static films to establish a continuous process for the production of a polymer resin. Hence, using a narrow channel reactor with a continuous flow would minimize the penetration depth which is essential for achieving narrow molecular weight distribution.[6] Efficient heat transfer in a microreactor has been a subject of interest for obtaining polymer with tighter molecular weight distribution and has been found to be more significant with highly exothermic polymerizations.[3]

A continuous photochemical reactor for production of vinyl polymers using a rotating spiral conveyer was developed by Kuriyama.[7] Although conversions up to 90% have been reported, the polymerization times were in the range of 6 h and the polydispersity indices of the polymer were also not mentioned to compare the quality of the polymer produced. A stationary cylindrical reactor for photopolymerization was developed by Berthold et al.[8] A UV lamp was installed in the center, and reactants were made to flow along the wall of the reactor concentric to the lamp. It was demonstrated that this reactor can be used to perform bulk, solution, and emulsion type polymerizations. In reactors with a free liquid surface, it is hard to maintain uniform film thickness, as the viscosity varies along the length of the reactor. Hence, the study of various parameters on the kinetics of polymerization will not be accurate. Continuous photopolymerization in a narrow channel flow system has been reported by Hicks and Melville to synthesize block copolymers.[9] A channel diameter of 1 mm and length of 30 cm was used. A length of 4 cm was used as the zone of illumination. Polymer chains initiated from the illuminated section would flow into a reservoir containing another monomer which would then propagate and eventually terminate. The conversions obtained in the process were very low, and the goal was to obtain linear block copolymers.

The objective of this work is to study photopolymerization of *n*-butyl acrylate using a narrow channel reactor system. This will combine the advantages of using continuous reactors with smaller dimensions and also the unique advantages of photopolymerization. The influence of photoinitiator concentration, intensity, and exposure time on conversion and molecular weights were studied. A mathematical model based on the kinetics of the polymerization in a static film was employed. In optically thin films, the predictions by Decker et al. suggest that the rate of polymerization is proportional to the square root of the intensity.[4] For optically thick films, the variation in the intensity is more significant and hence kinetic models that include spatial variation in intensity and local initiator concen-

* To whom correspondence should be addressed.

10.1021/ma071625l CCC: $40.75
Published on Web 04/09/2008

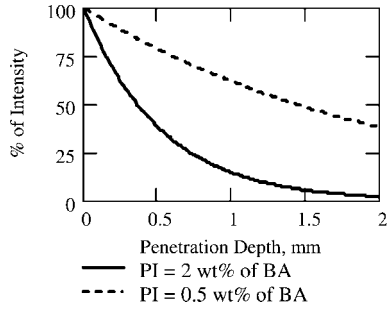

Figure 1. Variation of light intensity in the reactor due to absorption by photoinitiator (PI) species.

tration have been developed to predict the nonuniformity of the polymer cure with depth.[5,10–13] Interestingly, most of the theoretical work reported so far used photobleaching initiators. The effect of temperature on the rate constants has been taken into account. This has been done by calculating the rate constants to the corresponding exit temperature using the Arrhenius equation. The geometry of the channel was included in the model, since the circular cross section causes nonuniformity in the penetration of light through the reactor. Experimental results have been compared with the predicted values from the mathematical model developed.

2. Mathematical Model

A mathematical model has been developed for predicting the monomer conversion for different operating conditions. The geometry of the reactor is taken into account since penetration of light into the reactor, especially in the orders of millimeters, has a significant effect on the kinetics. Figure 1 shows the variation of light intensity with penetration depth based on Beers law assuming constant light absorbing species concentration across the path length. The photoinitiator used in this work is 2,2-dimethoxy-2-phenylacetophenone which has an absorption coefficient value, α, of 345 $L \cdot mol^{-1} \cdot cm^{-1}$.[14,15] The solid and dashed lines represent the variation of intensity for a photoinitiator concentration of 2% w/w monomer and 0.5% w/w monomer, respectively. The proposed model incorporates changes in UV intensity due to the variable path length resulting from the curved surface of the reactor. The exit temperatures from the experiments have been used to obtain the temperature profile along the length of the reactor. The temperature profile obtained has been used in the model to estimate the kinetic rate constants.

The expression used to predict the monomer conversion is given by:

$$\frac{d[\bar{X}]}{dt} = \left(\frac{k_{p1}}{\frac{\delta k_{bb}}{k_{p2}[M]_0(1-[\bar{X}])} + 1} + k_{tr,M} \right)(1-[\bar{X}]) \sqrt{\frac{2\phi_i \alpha [\bar{C}] I_0}{k_t}} (\bar{F}) \quad (2.1)$$

where

$$\bar{F} = \frac{2}{\pi R^2} \int_{r=0}^{r=R} \left[\left\{ \int_{\theta=3\pi/2}^{\theta=0} f(l_I(r,\theta)) r \, d\theta \, dr \right\} + \left\{ \int_{\theta=0}^{\theta=\pi/2} f(l_{IV}(r,\theta)) r \, d\theta \, dr \right\} \right] \quad (2.2)$$

Equation 2.1 is based on the model explained in Appendices A and B. The coefficients used have also been presented in detail. In the equation, $f(l) = (e^{(-\alpha l[\bar{C}])})^{1/2}$, $[\bar{C}] = [P]_0 e^{\phi_i \alpha I_0 t}$ and $[P]_0$ is the initial concentration of photoinitiator in the feed. The terms $\bar{F}$ and δ have been included in eq 2.1 to account for the geometry of the reactor and for the influence of the mixing/hydrodynamics on the kinetics. On the basis of the branching of 1.08 for 100 repeating monomer units, a δ ($\delta = k_{bb,exp}/k_{bb,0}$) value of 0.26 was obtained. It must be noted that a δ value of 0.26 has been obtained for a photoinitiator concentration of 2.0% w/w BA, intensity of 86 mW/cm^2, and exposure time of 24 s. For accurate prediction of experimental results pertaining to other photoinitiator concentrations, and experimental conditions, it is recommended to estimate and use the appropriate value of δ using the procedure described in Appendix A.

The model is based on the following assumptions: (a) plug flow behavior in the reactor, (b) propagation, termination mechanisms are independent of chain length, (c) temperature variation along the cross section of the reactor is negligible, (d) the primary radicals generated have equal mobility and reactivity, and (e) the concentration of light absorbing species, $[\bar{c}]$, is a function of time.

3. Experimental Section

3.1. Description of the Experimental Setup. The experimental setup consisted of a narrow channel reactor made of borosilicate with a wall thickness of 6.0 mm. The reactor which can be seen in Figures 2 and 3 has an approximate length of 900 mm and an internal diameter of 1.5 mm. The reactor has 10 linear sections each of 70 mm length and 9 semicircular bends with a radius of 7 mm. Ultraviolet radiation was generated by using a 400 W metal halide flood lamp supplied by Dymax Corporation. The UV flood lamp has a maximum intensity at 365 nm which is also the excitation wavelength of the initiator.[14] The lamp was supported by clamp stands in a manner such that the distance between the lamp and the reactor surface could be altered in order to study the influence of UV intensity on the reaction kinetics. The intensity of the UV radiation received on the reactor was measured by using a UV-A radio meter (model Accucal 20 series) from Dymax with an accuracy of ±2%. A gear pump was used to deliver the desired

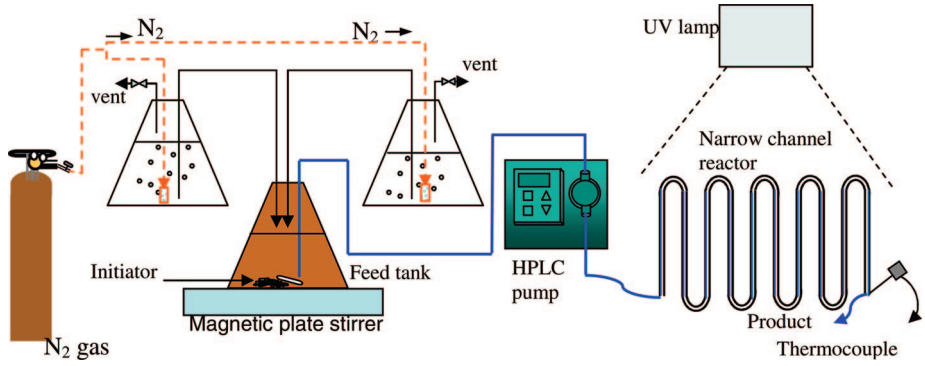

Figure 2. One detailed schematic of the experimental setup.

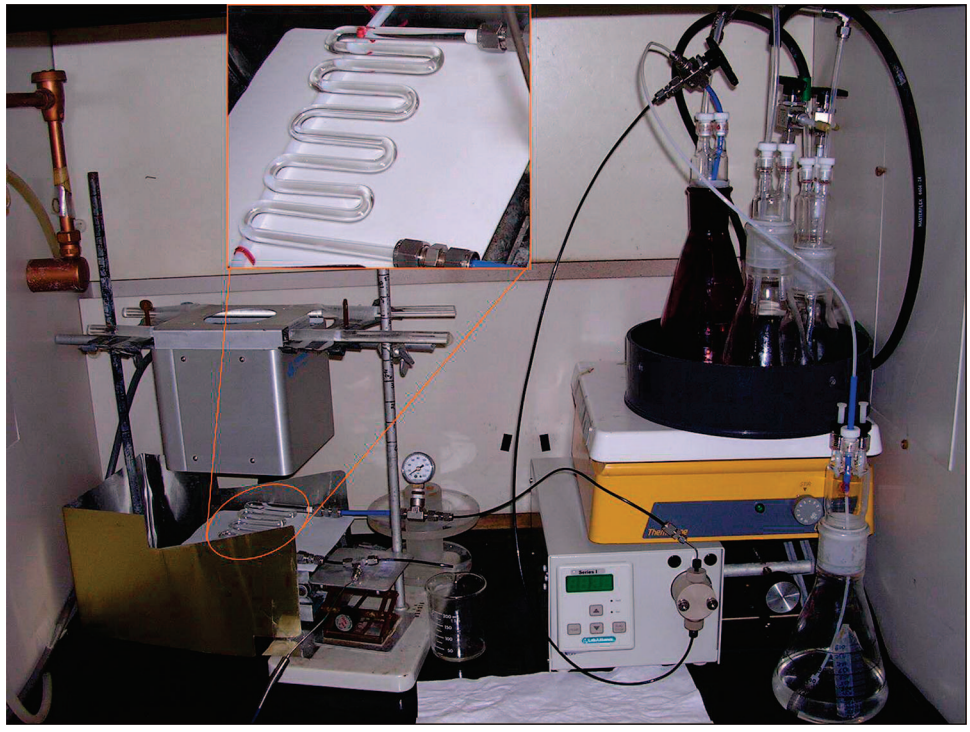

Figure 3. Photograph of the experimental setup.

reactant flow rate (25−70 mL/min) for the purpose of studying the influence of space time (3.8–1.36 s) on the reaction. The performance of a gear pump decreases at high viscosities obtained due to high conversions; hence, it is replaced with an HPLC pump (model C-74930-00) from Cole-Parmer for smaller flow rates. A thermocouple was used to measure temperature at the outlet of the reactor. The temperature profiles with time were recorded using a thermocouple−computer interface (Pico Technology Limited). Polymerization of *n*-butyl acrylate is an exothermic reaction; hence, the time–temperature profile was used to identify the steady state conditions in an experiment. Samples were collected for each experiment only when the system was under steady state conditions.

A fairly extensive arrangement was made in order to ensure the feedstock was free of oxygen. It was found that about 20 min was sufficient to effectively purge the system free of oxygen. As shown in Figure 2, the monomer and solvent were purged separately in Erlenmeyer flasks for 20 min and then fed to another Erlenmeyer flask which contains a premeasured amount of initiator. The transfer of the monomer and solvent was done by controlling/closing the exit valve of nitrogen in order to develop a positive pressure on the liquid. This approach was employed to ensure that the composition in the feed does not change due to loss of solvent and monomer by vaporization during the purging process. The preloaded initiator, monomer, and solvent were mixed for about 20 min using a magnetic stirrer. All of the experiments were carried out with 20% toluene by volume.

3.2. Chemicals Used. The monomer, *n*-butyl acrylate (Aldrich), was passed through an inhibitor remover column (Aldrich packed columns, 306312). Toluene, 2,2-dimethoxy-2-phenyl-acetophenone, and hydroquinone were obtained from Aldrich. Tetrahydrofuran obtained from J.T.Baker was used to dissolve the hydroquinone, and the solution was added to the product collected from the experiments to quench any unreacted radicals. Oxygen-free grade nitrogen was used for purging the feed mixture.

3.3. Characterization. A gas chromatograph (GC) was used for detection of monomer in the sample. Conversion is obtained by measuring the monomer peak area in the feed and product. An HP 5890 series II GC equipped with a flame ionization detector (FID) was used.

A gel permeation chromatography (GPC) system (PL-GPC 50; 2 × PL ResiPore (300 × 7.5 mm) columns; refractive index (RI) detector) from Polymer Laboratories (PL) was used for obtaining the molecular weight distribution of the product. The oven was maintained at a constant temperature of 30 °C. Tetrahydrofuran (THF) was used as a solvent at a flow rate of 1 mL/min. The molecular weights of the polymer were obtained by comparing against a calibration curve generated using poly(methyl methacrylate) (PMMA) narrow standards. Samples for GPC were made by dissolving 200 μL of sample in 5 mL of THF. About 500 μL of the diluted sample was then injected, and the chromatogram obtained was analyzed for the molecular weight distribution. Mark–Houwink parameters ($K = 12.2 \times 10^{-5}$ dL/g and $a = 0.70$) for poly(butyl acrylate) reported by Beuermann et al.[16] were used to estimate the absolute average molecular weights from the SEC curve.

4. Results and Discussion

4.1. Influence of Photoinitiator Concentration on Conversion and Molecular Weight. Parts a−c of Figure 4 show the variation of conversion as a function of initial photoinitiator concentration, $[P]_0$. The data points were obtained from the experiments, and the solid lines were obtained from the model. By using an UV intensity of 86 mW/cm^2, experiments were carried out for exposure times of 9.5, 11.9, and 15.9 s. Exposure times were varied by changing the flow rates. For the experiments studied at different exposure times, an optimum $[P]_0$ concentration of about 2.0% w/w monomer was observed to yield maximum monomer conversion. This finding is similar to that obtained by Boodhoo et al. in their investigation of *n*-butyl acrylate bulk photopolymerization in static films in the range of 200 μm to 1 mm.[5] For $[P]_0$ values higher than 2.5% w/w BA, primary radical termination is believed to be the possible cause for the decrease in conversion. When the local concentration of the radicals is high, the radicals terminate bypassing the propagation step to yield dead fragments.[9,15] When the $[P]_0$ concentration was less than 2% w/w BA, the amount of polymer formed increased with an increase in the amount of the $[P]_0$ used. Since a $[P]_0$ value of 2% w/w BA was found to be the optimum, the same was chosen for experiments to study the influence of exposure times and light intensity.

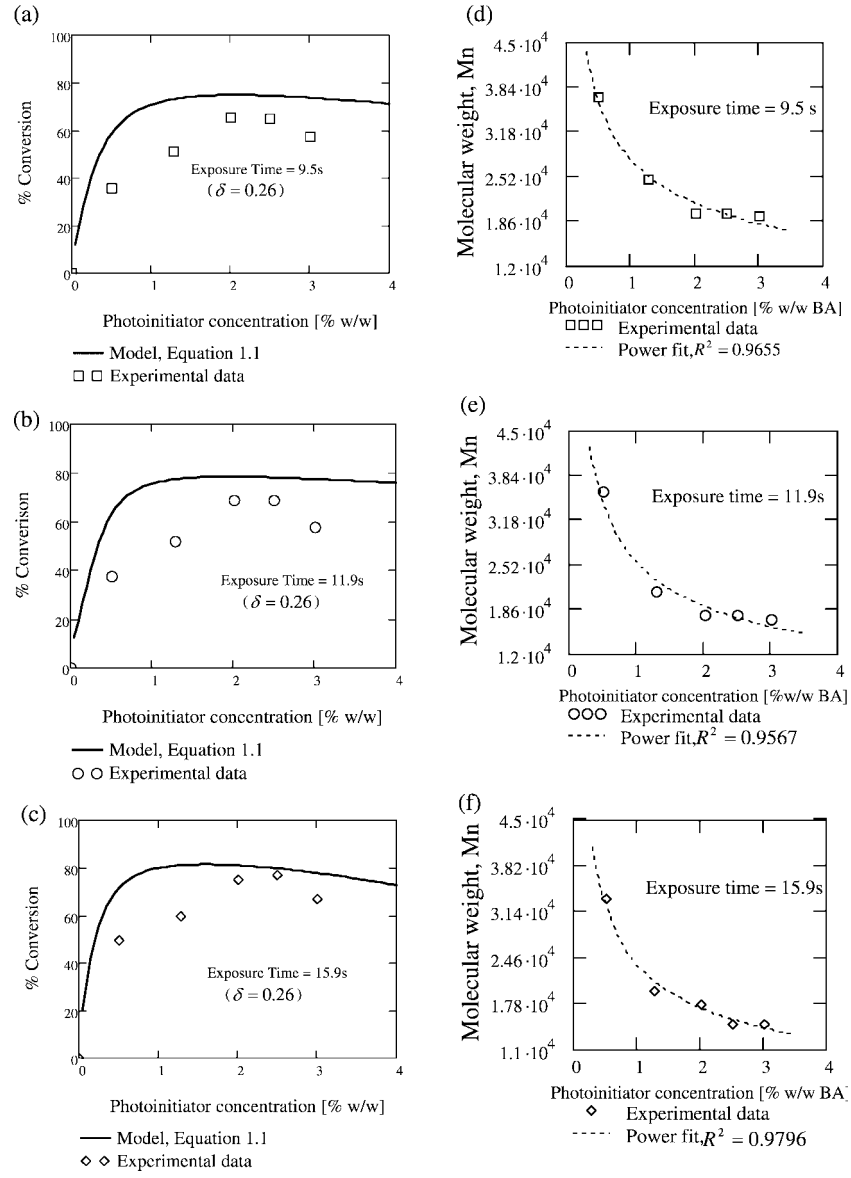

Figure 4. Influence of initiator concentration on conversion and molecular weights.

Table 1. Effect of Initial Photoinitiator Concentration on PDI of the Polymer

$[P]_0$, % w/w BA	range of BA conversion, %	molecular weights, $\bar{M}_n \cdot 10^{-3}$	PDI ($\bar{M}_w/\bar{M}_n$)	exit temperatures, °C
0.5	35–50	33.8–36.9	1.7–1.9	80–90
1.3	51–81	14.9–24.6	1.8–2.2	66–118
2.0	18–81	12.4–28.6	2.0–2.6	87–130
2.5	65–77	16.5–19.8	2.0–2.7	100–125
3.0	57–76	14.8–19.2	1.9–2.3	95–125

When the photoinitiator concentration, $[P]_0$, is 2% w/w BA, there is a good fit between the experimental and model predicted values. This is because the $k_{bb,exp}$, the rate constant for backbiting, value used in the model was experimentally obtained for a $[P]_0$ value of 2% w/w BA. In order to improve the model so that there is an improved fit between the model and the experimental values, it is essential to experimentally obtain $k_{bb,exp}$ values for the corresponding $[P]_0$ values.

Parts d−f of Figure 4 show the variation of molecular weight as a function of $[P]_0$. The data points were obtained from the experiments, and the dashed lines were obtained by fitting a curve to the experimental data points. It can be seen that the molecular weight decreases with an increase in initiator concentration. It was also observed that the polydispersity indices (PDI) increased with an increase in initiator concentration, as shown in Table 1.

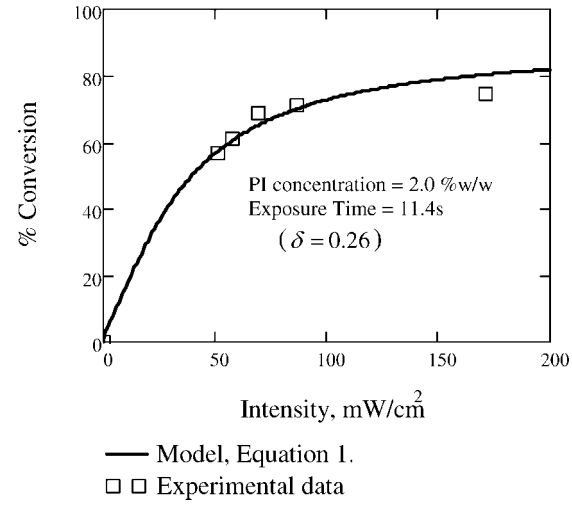

Figure 5. Influence of UV intensity on conversion.

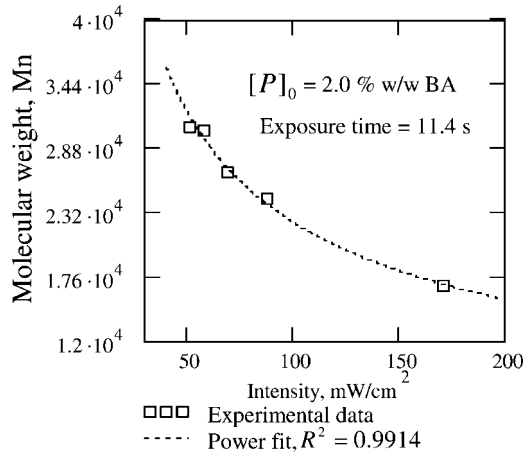

Figure 6. Influence of intensity on molecular weight.

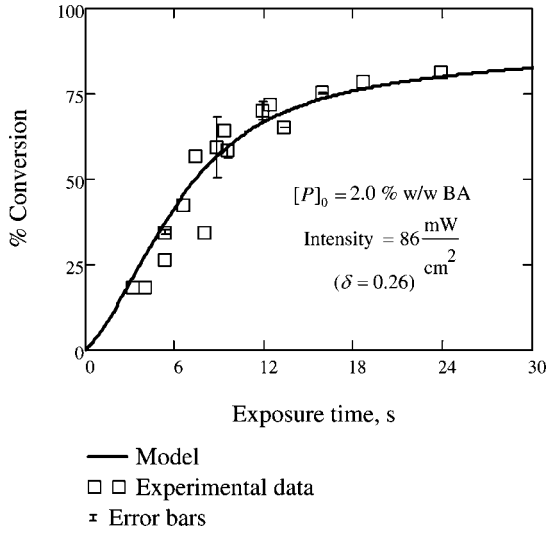

Figure 7. Influence of exposure time on conversion.

As seen in Table 1, the PDI values increase as $[P]_0$ increases from 0.5 to 2.0%. Beyond the 2.0% value, the PDI is seen to stabilize. As explained by Terrnones et al.,[13] this is attributed to the increase in nonuniform rates of initiation as $[P]_0$ increases. According to Beer's law, more light is absorbed at high concentrations of the photoinitiator species. Hence, increased photoinitiator concentration shields the incident light from reaching the bottom of the reactor (Figure 1).

4.2. Influence of Intensity on Conversion and Molecular Weight. Figure 5 shows the variation of conversion as a function of UV light intensity. Experiments were performed for a fixed $[P]_0$ value of 2% w/w and an exposure time of 11.4 s. The UV intensity was varied by changing the height of the lamp from the reactor surface. It is found that the conversion increases with an increase in the intensity. In the range of light intensities studied, the model predicts the experimental findings.

Figure 6 shows the variation of molecular weight with light intensity. The molecular weight of the polymer formed decreased with an increase in intensity. At higher intensities, the radical concentration increases, resulting in a decrease of the molecular weight.

4.3. Influence of Exposure Time on Conversion and Molecular Weight. Figure 7 shows the influence of exposure time on monomer conversion. For all of the experiments performed, the exposure time is the same as the space time. Different exposure times were obtained by varying the flow rate of the feed. A constant $[P]_0$ concentration of 2.0% w/w and intensity of 86 mW/cm^2 were maintained in the experiments. As expected, the initial increase in the conversion was high and the slope decreased slowly, which corresponds to a reduced rate of polymerization. It is known that the conversion is a function of monomer concentration, initiator concentration, and temperature. Therefore, as the polymerization proceeds along the length of the reactor, the monomer and initiator concentrations decrease, resulting in a decrease in the rate of conversion.

Along the length of the reactor, exposure time varies and hence the temperature. As kinetic constants depend on temperature, it is essential to know the temperature profile along the length of the reactor for different exposure times. As temperature can be measured only at the exit for any given reactor length, experiments were carried out to study the influence of exposure time by changing the flow rate through a 90 cm long reactor. The exit temperatures for the above study have been shown in Figure 8a. A series of experiments were also carried out using reactor lengths of 70, 50, and 30 cm. The temperatures obtained are shown in Figure 8b. It can be seen that, for nearly equal exposure times (obtained with different lengths of reactor and different flow rates), the outlet temperatures are nearly equal. Hence, it can be assumed that

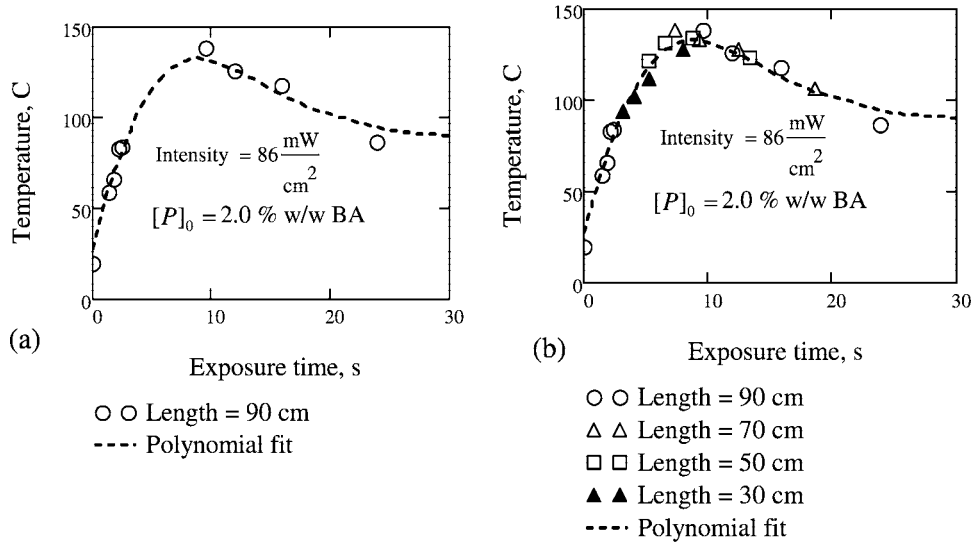

Figure 8. Influence of exposure time on the steady state temperatures.

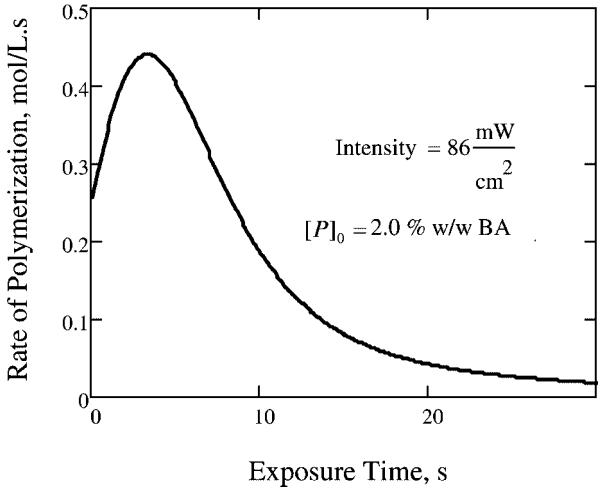

Figure 9. Influence of exposure time on rate of polymerization.

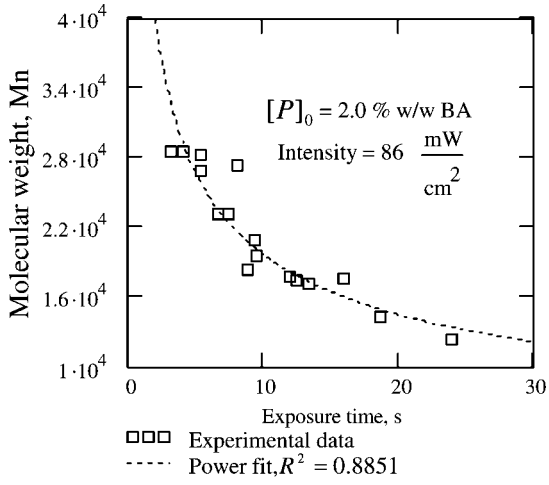

Figure 10. Influence of exposure time on molecular weight.

the temperature profile along the length of the reactor can be deduced if the exposure times are known. The time–temperature data have been used to obtain a polynomial fit for establishing a continuous time dependent function for integrating eq 2.1 to predict monomer conversions. Similar temperature profiles for predicting monomer conversions were also obtained as a function of light intensity and initiator concentrations.

It is found that there is a peak temperature corresponding to the exposure time suggesting that the rate of polymerization will initially increase and then decrease. A similar trend for rate of polymerization (Figure 9) has been obtained by using the model which uses the temperature profile data (Figure 8).

As seen in Figure 7, there is a good fit between the conversion values obtained theoretically to those obtained experimentally.

Figure 10 shows the influence of exposure time on the molecular weight of the polymer formed. It can be seen that the molecular weight of the polymer decreases with an increase in exposure time. A longer exposure time generates more photons which in turn increases the radical concentration. Therefore, the number of competing propagating chains is increased, resulting in polymers with shorter chains. For smaller exposure times, the number of radicals initiated was low and hence polymers with high molecular weights were obtained.

NMR analysis on a sample was performed, and the NMR spectra obtained can be seen in Figure 11. The following experimental conditions were maintained for the sample analyzed: exposure time, 25 s; intensity, 86 mW/cm^2; $[P]_0$, 2% w/w BA.

The degree of branching has been estimated from the ratio of the sum of the branched CH and CH_2 integrals (peaks B and C in Figure 11) to the total integral for backbone carbon atoms (peaks A and D in Figure 11).[17,18] On the basis of the NMR findings, an average value of 1.08 has been used as the amount of branches per 100 repeat backbone units. As detailed in Appendix A, δ has been calculated using the branching data.

4.4. Comparison of Thermal Polymerization and Photopolymerization. In Table 2, an attempt has been made to compare the experimental results obtained with published data on thermal polymerization of *n*-butyl acrylate. Thermal polymerization data based on batch and microreactor configurations, with 2,2′-azo-bis(isobutyronitrile) (AIBN) as the initiator, were obtained from Iwasaki et al.[3] For conversions in the range 81–87%, it can be seen from Figure 12 that significant reduction in reaction time can be achieved by using the photopolymerization technique in a narrow channel reactor system. The time savings is approximately 3 and 4 times compared to thermal polymerization in a microreactor and batch reactor, respectively. This effect is due to the high rates of initiation in photopoly-

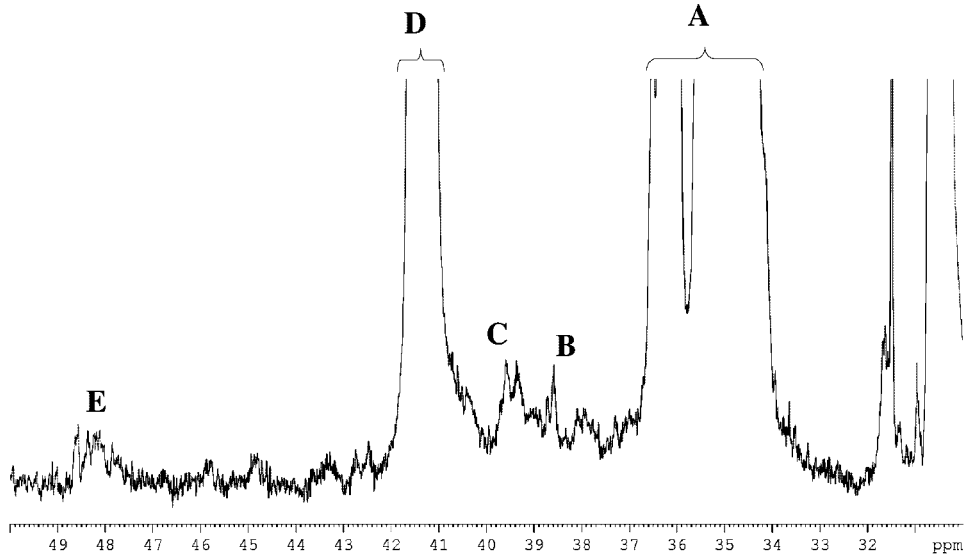

Figure 11. NMR spectra with assigned peaks to estimate branching in PBA.

Table 2. Comparison of Polymerization Kinetics by Different Schemes (Based on Initiator Concentration = 1 mol % of BA)

reactor	space time/ exposure time, s	conversion, *X*%	molecular weight, $\bar{M}_n \cdot 10^{-3}$	PDI ($\bar{M}_w/\bar{M}_n$)
thermal macroscale	120.0	50.0	27.1	212.00
batch reactor feed, 50% v/v; temp, 100 °C (3)	180.0	82.1	10.0	9.61
	210.0	86.0	9.3	10.00
	240.0	88.0	9.3	10.30
thermal microreactor	90.0	72.4	33.0	3.63
temp, 100 °C; feed, 50% v/v; diameter, 0.5 mm (3)	120.0	86.5	26.1	3.59
	180.0	86.5	22.8	3.14
	240.0	89.6	20.8	3.16
	300.0	89.3	19.2	3.35
photopolymerization	9.5	51.1	24.6	2.61
nonisothermal; feed, 80% v/v; diameter, 1.5 mm	10.6	52.2	23.2	2.12
	11.9	51.7	21.3	1.77
	13.6	58.4	20.6	1.79
	15.9	59.8	19.7	1.99
	19.1	68.5	18.7	1.92
	38.2	81.4	14.9	2.03

merization. The high rates of initiation become significant in curing applications where the excess free volume provides increased mobility for species improving the overall rate of polymerization.[4,19] It can also be seen from Figure 13 that the PDI achieved using photopolymerization in a narrow channel is lower than that achieved by thermal polymerization. It should be highlighted that the amount of solvent used by Iwasaki et al. was 50% v/v, while this work was carried out with a solvent of 20% v/v. It is to be expected that the use of an increased amount of solvent will yield lower PDIs as the viscosity of the reacting medium is reduced. In continuous flow photopolymerization, the exothermic nature of the acrylate polymerization and the heat from the lamp will provide better mixing of the radicals generated. Higher temperatures during the reaction will decrease the viscosity, and this will enhance mixing inside the channel.

Flow through narrow channels is known to provide very good convective heat transfer rates. This will result in a uniform temperature distribution within the polymer across a given flow cross section. The high rates of initiation associated with photo-

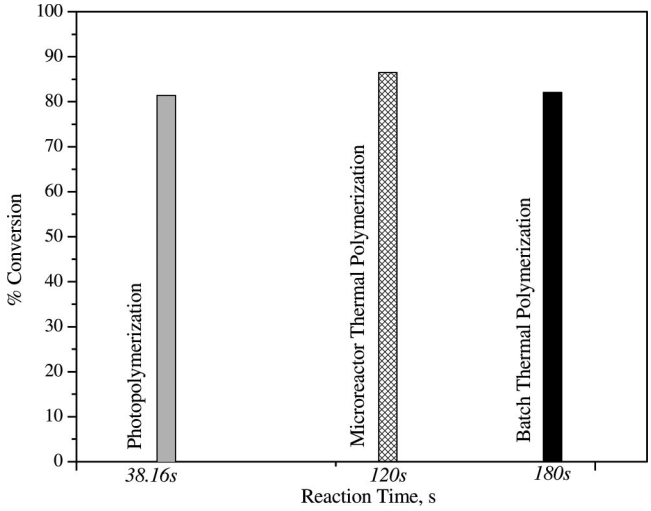

Figure 12. Comparison for reaction times: photopolymerization vs thermal polymerization.

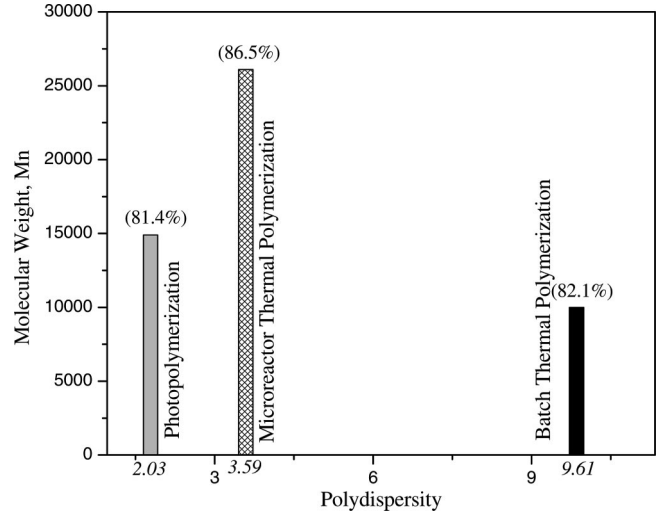

Figure 13. Comparison of polydispersity indices: photopolymerization vs thermal polymerization (conversion values are given in parentheses).

Table 3. Arrhenius Rate Coefficients Used in the Model

$k_{p1} = 2.05 \times 10^7 \exp(-17890/RT)$	$lit \cdot mol^{-1} \cdot s^{-1}$	ref 28[a]
$k_{p2} = 1.25 \times 10^6 \exp(-29500/RT)$	$lit \cdot mol^{-1} \cdot s^{-1}$	ref 29
$k_{tr,M} = 2.9 \times 10^5 \exp(-32600/RT)$	$lit \cdot mol^{-1} \cdot s^{-1}$	ref 30
$k_{bb,0} = 3.5 \times 10^7 \exp(-29300/RT)$	s^{-1}	ref 28
$k_t = 2.57 \times 10^8 \exp(-5590/RT)$	$lit \cdot mol^{-1} \cdot s^{-1}$	ref 22

[a] A recent publication by Pierik et al.[31] reported $k_{p1} = 1.0 \times 10^7 \exp(-15900/RT)$ $L \cdot mol^{-1} \cdot s^{-1}$. The effect of branching has been neglected by using high pulse frequencies in their estimation, but Plessis et al.[28] have included the branching in their estimation of the kinetic rate constant and it was therefore used in this work.

polymerization coupled with narrow temperature distribution may have resulted in the lower PDIs that were experimentally obtained.

5. Conclusions

An experimental setup was developed and tested for investigating free radical photopolymerization of *n*-butyl acrylate in a continuous flow mode using a narrow channel reactor. The influence of photoinitiator concentration, UV intensity, and exposure times on monomer conversion and molecular weights has been studied. It was found that a photoinitiator concentration of 2% w/w monomer provided the highest monomer conversion in the range of UV intensities and exposure times investigated. The PDIs of the polymer obtained increased with initiator concentration up to 2% w/w BA. The results of this investigation when compared with thermal polymerization studies have shown that the kinetics are faster for photoinitiated systems and the PDIs of the polymer obtained were lower than those obtained by thermal polymerization. A theoretical model to predict the monomer conversions which incorporates the geometry of the reactor has been developed. NMR study indicated a branching of 1.08% in one of the products analyzed.

Acknowledgment. The authors would like to acknowledge the contributions made by late Dr. W. A. E. Dunk, Dr. D. Shipp, and P. K. Chintamanipeta (NMR analysis) and the financial support from NYSTAR (New York State office of Science, Technology & Academic Research) toward this work.

Appendix A: Mathematical Model Development

The following kinetic mechanisms were considered in the development of the model. In addition to the classical free radical mechanisms, secondary reactions have also been included. The secondary reactions are more predominant at higher temperatures and at lower monomer concentrations.[20–23]

Initiation:

$$P \xrightarrow{h\nu} 2R\bullet \quad (A.1)$$

$$R\bullet + M \xrightarrow{k_{p1}} R_1\bullet \quad (A.2)$$

Propagation:

$$R_n\bullet + M \xrightarrow{k_{p1}} R_{n+1}\bullet \quad (A.3)$$

$$R_n^*\bullet + M \xrightarrow{k_{p2}} R_{n+1}\bullet \quad (A.4)$$

Chain Transfer to Monomer:

$$R_n\bullet(R_n^*\bullet) + M \xrightarrow{k_{tr,M}} M_n + R_1\bullet \quad (A.5)$$

Intramolecular chain transfer to polymer, backbiting:

$$R_n\bullet \xrightarrow{k_{bb}} R_n^*\bullet \quad (A.6)$$

Intermolecular chain transfer to polymer:

$$R_n\bullet + M_m \xrightarrow{k_{tr,p}} M_n + R_m^*\bullet \quad (A.7)$$

Termination by combination:

$$R_x\bullet + R_y\bullet \xrightarrow{k_{t11}} M_{x+y} \quad (\text{or } M_p + M_q) \quad (A.8\text{-}1)$$

$$R_x\bullet + R_y^*\bullet \xrightarrow{k_{t12}} M_{x+y} \quad (A.8\text{-}2)$$

$$R_x^*\bullet + R_y^*\bullet \xrightarrow{k_{t22}} M_{x+y} \quad (A.8\text{-}3)$$

$$R_x\bullet(R_x^*\bullet) + R_y\bullet(R_y^*\bullet) \xrightarrow{k_t} M_{x+y} \quad (A.8)$$

In the above expressions, P represents the photoinitiator, M is monomer, R• is a free radical, R_n• represents a growing polymer radical with n repeating units, R_n^* represents a tertiary radical formed either by the backbiting process (eq A.6) or by intermolecular chain transfer to another polymer (eq A.7), and M_{x+y}, M_p, M_m, M_n, and M_q represent dead polymer chains formed containing $x + y$, p, m, n, and q repeating units, respectively.

h and ν represent Planck's constant and the frequency of light, respectively. $h\nu$ represents a quantum of light absorbed by the photoinitiator to generate the primary radicals. In the model, the frequency corresponding to a wavelength of 365 nm was used. k_{p1} and k_{p2} represent the rate constant of propagation for secondary and tertiary radicals, respectively. $k_{tr,M}$, $k_{tr,p}$, k_{bb}, k_{t11}, k_{t22}, k_{t12}, and k_t represent rate constants for chain transfer to monomer, intermolecular chain transfer to polymer, backbiting, secondary radical termination, tertiary radical termination, cross radical termination, and overall radical termination, respectively. In *n*-butyl acrylate polymerization, it is known that termination by combination is more dominant over disproportionation. Termination can occur by combination of secondary or tertiary radicals (eqs A.8-1, A.8-2, and A.8-3). The combination of all of these reactions has been expressed in eq A.8, where k_t represents the combined rate constant for termination of all of the radicals.

Table 4. Parameters Used in the Model

ϕ_i: quantum yield of initiation for DMPA	0.6	ref 10
α: molar absorptivity of DMPA	345 lit·mol^{-1}·cm	ref 10
λ: wavelength of UV light	365 nm	
L: length of the reactor	90 cm	
d: diameter of the reactor	0.15 cm	
V: volume of the reactor, $[(\pi/4)d^2L]$	1.59 cm^3	
t: space time or exposure time, $[V/Q]$	S	
Q: volumetric flow rate	2.5–70 mL·min^{-1}	
$[M]_0$: initial concentration of BA	5.61 mol·lit^{-1}	
$[S]$: concentration of toluene (20% v/v)	1.88 mol·lit^{-1}	

Chain transfer to polymer occurs by two mechanisms: Intermolecular chain transfer that yields long chain branches (LCBs) and intramolecular chain transfer that yields short chain branches (SCBs). SCBs are formed by propagation of tertiary radicals formed by the backbiting phenomenon. The backbiting mechanism is considered to occur by size-membered-ring transition. Intermolecular chain transfer reaction has been neglected, so the branching polymer is associated to the backbiting phenomenon only. Former et al. have reported the dominance of SCBs over LCBs based on the viscoelastic behavior of the polymer.[24] It was assumed that the tertiary radicals do not undergo intermolecular chain transfer reactions. The tertiary radicals also undergo β-scission to yield a dead polymer chain with a terminal double bond and a live polymer chain.[17,25,26] This mechanism is found to be dominant at high temperatures and affects the PDI of the polymer more than the monomer conversion. Hence, it is neglected in this kinetic model.

Intermolecular chain transfer by secondary radicals to polymer was also neglected. The kinetic expression for the rate of polymerization has been derived on the basis of the assumption that backbiting is the predominant chain transfer event.

The rate of monomer conversion, r_m, can be estimated from eqs A.3, A.4, and A.5 as follows:

$$r_m = (k_{p,eff} + k_{tr,M})[M][R_n^{sum}\bullet] \quad (A.9)$$

In the above equation, R_n^{sum}• is the total concentration of radicals (secondary and tertiary). $k_{p,eff}$ is the effective rate constant of propagation and can be used in place of the traditional rate constant for propagation, k_p.[21,27] It is defined as follows:

$$k_{p,eff} = \frac{k_{p1}}{\frac{\delta k_{bb,0}}{k_{p2}[M]} + 1} \quad (A.10)$$

The expression for $k_{p,eff}$ given in eq A.10 is valid under the assumption that backbiting is the predominant chain transfer mechanism affecting the kinetics. δ is the ratio of $k_{bb,exp}$ obtained from the experiment and $k_{bb,0}$ obtained by Plessis et al.[28] $k_{bb,exp}$ is estimated from the degree of branching using the following expression:

$$\text{Branching} = \frac{k_{bb,exp}}{[k_{p1}[M]_0(1-X)] + k_{bb,exp}} \quad (A.11)$$

Rate of initiation:

$$r_i = 2\phi_i\alpha[\bar{C}]I_0 e^{-\alpha l[\bar{C}]} \quad (A.12)$$

Rate of termination:

$$r_t = 2k_t[R_n^{sum}\bullet]^2 \quad (A.13)$$

r_i and r_t represent the rate of initiation and rate of termination, respectively. ϕ_i is the quantum yield of initiation; l is the penetration depth of light; I_0 is the intensity of light on the

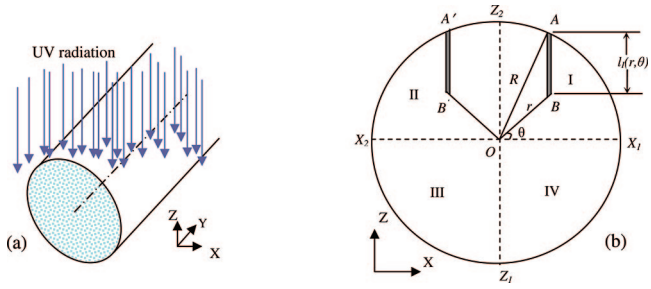

Figure 14. (a) Schematic of the reactant under UV radiation and (b) a cross-sectional view of the reactor.

surface of the reactor; α is the absorption coefficient of the light absorbing species (it is assumed that the primary radicals and photoinitiator molecules have the same absorption coefficient); $[\bar{C}]$ is the concentration of the light absorbing species across the cross section. For DMPA, a nonphotobleaching initiator, the light absorbing species consist of unreacted photoinitiator molecules and primary radicals in the system. The average concentration of the light absorbing species is assumed to be constant for the cross section and has been given as $[\bar{C}] = [\mathrm{P}]_0 \mathrm{e}^{\phi_i \alpha I_0 t}$.[5] This expression has been obtained by using a thin film approximation and is more realistic for films in the order of microns.[1] $[\mathrm{P}]_0$ is the initial concentration of photoinitiator.

Using the quasi-steady-state assumption on radicals ($r_i = r_t$), eqs A.12 and A.13 lead to

$$[\mathrm{R}_n^{\mathrm{sum}}\bullet] = \sqrt{\frac{\phi_i \alpha [\bar{C}] I_0 \mathrm{e}^{-\alpha l [\bar{C}]}}{k_t}} \tag{A.14}$$

In this expression, $(\mathrm{e}^{(-\alpha l[\bar{C}])})^{1/2}$ is a function of l. As shown in Figure 14a, the light penetration into the reactor is nonuniform due to the geometry of the reactor which leads to nonuniform penetration of light across the sample cross section. The average value of this expression for the cross section of the reactor can be obtained on the basis of the derivation given in Appendix B (eq B.5).

The rate of monomer consumption can be estimated from eqs A.9 and A.14 as follows:

$$r_m = -\frac{\mathrm{d}[\overline{\mathrm{M}}]}{\mathrm{d}t} = \left(\frac{k_{p1}}{\dfrac{\delta k_{bb,0}}{k_{p2}[\mathrm{M}]} + 1} + k_{tr,M}\right)[\mathrm{M}]\sqrt{\frac{\phi_i \alpha [\bar{C}] I_0 \mathrm{e}^{-\alpha l [\bar{C}]}}{k_t}} \tag{A.15}$$

In eq A.15, if we define $f(l) = (\mathrm{e}^{(-\alpha l[\bar{C}])})^{1/2}$ and $\bar{F}$ as the average value across the circular cross section, then eq A.15 can be rewritten in terms of $\bar{F}$ as follows:

$$r_m = -\frac{\mathrm{d}[\overline{\mathrm{M}}]}{\mathrm{d}t} = \left(\frac{k_{p1}}{\dfrac{\delta k_{bb,0}}{k_{p2}[\overline{\mathrm{M}}]} + 1} + k_{tr,M}\right)[\overline{\mathrm{M}}]\sqrt{\frac{\phi_i \alpha [\bar{C}] I_0}{k_t}}(\bar{F}) \tag{A.16}$$

Monomer conversion, $\bar{X}$, can be obtained by

$$\bar{X} = 1 - \frac{[\overline{\mathrm{M}}]}{[\mathrm{M}]_0} \tag{A.17}$$

Equations A.16 and A.17 can be used to estimate the monomer conversion as a function of exposure time, photoinitiator concentration, and light intensity. In the equations, $[\bar{C}]$ is assumed to be constant across the cross section. However, $[C]$, the local concentration of light absorbing species, can be expressed as a function of penetration depth l and time as derived by Terrones et al.[13] and the average value, $\bar{F}$, in eq A.16 can be calculated using the method described in Appendix B.

The heat of polymerization for *n*-butyl acrylate is about 500 kJ/kg. Hence, the exothermic nature of the reaction causes a significant increase in the temperature during polymerization. The experiments in this work were carried out without any provisions for removing the heat generated. However, there is loss of heat by convection of air around the reactor and hence the reaction conditions were described as nonisothermal and nonadiabatic. Therefore, the monitored exit temperature from the experiment is an important measure and was used to estimate the approximate values for the rate constants. For a given experiment, only one of the parameters (exposure time, concentration of photoinitiator, and light intensity) has been varied and the steady state exit temperatures were monitored. Hence, to predict the conversion from the model (eq 2.1) for any value of the parameter, the corresponding temperatures were used. A typical profile of steady state temperature as a function of exposure time is given in Figure 8.

Appendix B: Geometry Incorporation

The schematic and sectional views of the reactor under UV radiation are given in parts a and b of Figure 14, respectively. The direction of the flow is along the *Y*-axis. *R* is the radius of the reactor. Light penetrates the reactor from the top surface (semicircle $X_1-Z_2-X_2$ in the sectional view B.1 (b)) and travels to the bottom. l is the penetration depth of light to any point in the reactor. For a point *B* in the reactor, *A* is the point where light enters into the reactor and l is represented by *AB*. The penetration depth, l, in each of the quadrants is represented by l_I, l_{II}, l_{III}, and l_{IV} in quadrants I, II, III, and IV, respectively. l is expressed in polar coordinates r and θ. r is the distance of any point from the center "*O*" and θ is the angle subtended by the line connecting the point and center and OX_1 in the anticlockwise direction (e.g., for point *B*, θ is the angle between *OB* and OX_1). The reactor is symmetrical along the plane Z_1-Z_2. In the following section, the functions are derived for quadrants I and IV only.

All of the points in quadrants I and IV can be expressed in polar coordinates, and each point will have an independent penetration depth, l, given by

$$l_I(r,\theta) = -r\sin\theta + \sqrt{R^2 - (r\cos\theta)^2}; \quad l_{IV}(r,\theta) = r\cos\theta + \sqrt{R^2 - (r\sin\theta)^2} \tag{B.1}$$

For any point *B* ($r\cos\theta$, $r\sin\theta$) in quadrant I, there will be a point *B′* ($-r\cos\theta$, $r\sin\theta$) symmetrical in quadrant II. The penetration depth of light is the same from the top of the reactor to the points *B* and *B′*. Therefore, $l_I(r,\theta) = l_{II}(r,\theta)$ and $l_{IV}(r,\theta) = l_{III}(r,\theta)$.

For a function $f(l)$ which is continuous inside the circle (Figure 14b), the integrals of the function $f(l)$ in quadrants I and IV are given by

$$\int_{r=0}^{r=R}\int_{\theta=0}^{\theta=\pi/2} f(l_I(r,\theta))r\,\mathrm{d}\theta\,\mathrm{d}r$$

and

$$\int_{r=0}^{r=R}\int_{\theta=3\pi/2}^{\theta=2\pi} f(l_{IV}(r,\theta))r\,\mathrm{d}\theta\,\mathrm{d}r \tag{B.2}$$

Since $f(l)$ is symmetrical along the $Z1-Z2$ plane,

$$\int_{r=0}^{r=R}\int_{\theta=0}^{\theta=\pi/2} f(l_{\mathrm{I}}(r,\theta))r\,\mathrm{d}\theta\,\mathrm{d}r = \int_{r=0}^{r=R}\int_{\theta=\pi/2}^{\theta=\pi} f(l_{\mathrm{II}}(r,\theta))r\,\mathrm{d}\theta\,\mathrm{d}r \tag{B.3}$$

$$\int_{r=0}^{r=R}\int_{\theta=3\pi/2}^{\theta=2\pi} f(l_{\mathrm{IV}}(r,\theta))r\,\mathrm{d}\theta\,\mathrm{d}r = \int_{r=0}^{r=R}\int_{\theta=\pi}^{\theta=3\pi/2} f(l_{\mathrm{III}}(r,\theta))r\,\mathrm{d}\theta\,\mathrm{d}r \tag{B.4}$$

The average value of the function $f(l)$, given by $\bar{F}$, over the whole cross-sectional area is given by

$$\bar{F} = \frac{2}{\pi R^2}\int_{r=0}^{r=R}\left[\left\{\int_{\theta=3\pi/2}^{\theta=2\pi} f(l_{\mathrm{I}}(r,\theta))r\,\mathrm{d}\theta\,\mathrm{d}r\right\} + \left\{\int_{\theta=0}^{\theta=\pi/2} f(l_{\mathrm{IV}}(r,\theta))r\,\mathrm{d}\theta\,\mathrm{d}r\right\}\right] \tag{B.5}$$

References and Notes

(1) Oster, G.; Yang, N. Photopolymerization of Vinyl Monomers. *Chem. Rev.* **1968**, *68* (2), 125–151.
(2) Dunk, B. A.; Jachuck, R. J. J. A Novel Continuous Reactor for UV irradiated Reactions. *Green Chem.* **2000**, *2* (1), G13–G14.
(3) Iwasaki, T.; Yoshida, J. Free Radical Polymerization in Microreactors. Significant Improvement in Molecular Weight Distribution Control. *Macromolecules* **2005**, *38*, 1159–1163.
(4) Boodhoo, K. V. K.; Dunk, W. A. E.; Jassim, M. S.; Jachuck, R. J. J. Thin Film Solvent-Free Photopolymerization of *n*-Butyl acrylate. I. Static film studies. *J. Appl. Polym. Sci.* **2004**, *91*, 2079–2095.
(5) Wu, T.; Mei, Y.; Cabral, J. T.; Xu, C.; Beers, K. L. A New Synthetic Method for Controlled Polymerization using a Microfluidic System. *J. Am. Chem. Soc.* **2004**, *126* (32), 9880–9881.
(6) Decker, C. The use of UV Irradiation in Polymerization. *Polym. Int.* **1998**, *45*, 133–141.
(7) Kuriyama, A. Continuous Photochemical Reactor. U.S. Patent 4,849,183, **1989**.
(8) Keggenhoff, B.; Bandtel, E.; Rosenkranz, H. J. Use of an Apparatus for Continuous Photopolymerization. U.S. Patent 4, 211, 761, 1980.
(9) Hicks, J. A.; Melville, H. W. The Synthesis of Block Copolymers in a Flow System. *J. Polym. Sci.* **1954**, *12*, 461–468.
(10) Goodner, M. D.; Bowman, C. N. *Solvent Free Polymerizations and Processes. Minimization of Conventional Organic Solvents*; Long, T. E., Hunt, M. O., Eds.; ACS Symposium Series 713; American Chemical Society: Washington, DC, 1998.
(11) Miller, G. A.; Gou, L.; Narayanan, V.; Scranton, A. B. Modeling of Photobleaching for the Photoinitiation of Thick Polymerization Systems. *J. Polym. Sci., Part A: Polym. Chem.* **2002**, *40*, 793–808.
(12) Ivanov, V. V.; Decker, C. Kinetic Study of Photoinitiated Frontal Polymerization. *Polym. Int.* **2001**, *50*, 113–118.
(13) Terrones, G.; Pearlstein, A. J. Effects of Optical Attenuation and Consumption of a Photobleaching Initiator on Local Initiation Rates in Photopolymerization. *Macromolecules* **2001**, *34*, 3195–3204.
(14) Crivello, J. V.; Dietliker, K. Surface Coatings Technology. *Photoinitiators for Free Radical, Cationic and Anionic Photopolymerization*, 2nd ed.; John Wiley and Sons: New York, 1998; Vol. *III*.
(15) Goodner, M. D.; Bowman, C. N. Modeling of Primary Radical Termination and Its Effects on Autoacceleration in Photopolymerization Kinetics. *Macromolecules* **1999**, *32*, 6552–6559.
(16) Beuermann, S., Jr.; McMinn, J. H.; Hutchinson, R. A. Determination of Free-Radical Propagation Rate Coefficients of Butyl, 2-Ethylhexyl, and Dodecyl Acrylates by Pulsed-Laser Polymerization. *Macromolecules* **1996**, *29*, 4206–4215.
(17) Peck, A. N. F.; Hutchinson, R. A. Secondary Reactions in the High-Temperature Free Radical Polymerization of Butyl Acrylate. *Macromolecules* **2004**, *37*, 5944–5951.
(18) Ahmad, N. M.; Heaytley, F.; Lovell, P. A. Chain Transfer to Polymer in Free-Radical Solution Polymerization of *n*-Butyl Acrylate Studied by NMR Spectroscopy. *Macromolecules* **1998**, *31*, 2822–2827.
(19) Decker, C.; Decker, D.; Morel, F. Real-Time Temperature Monitoring in High-Speed Photopolymerization. *Polymeric Materials: Science and Engineering, Proceedings of the ACS Division of Polymeric Materials, Science and Engineering* **1996**, *74*, 350–351.
(20) Lyons, R. A.; Hutovic, J.; Piton, M. C.; Christie, D. I.; Clay, P. A.; Manders, B. G.; Kable, S. H.; Gilbert, R. G. Pulsed-Laser Polymerization Measurements of the Propagation Rate Coefficient for Butyl Acrylate. *Macromolecules* **1996**, *26*, 1918–1927.
(21) Asua, J. M.; Beuermann, S.; Buback, M.; Castignolles, P.; Charleux, B.; Gilbert, R. G.; Hutchinson, R. A.; Leiza, J. R.; Nikitin, A. N.; Vairon, J. P.; Herk, A. M. V. Critically Evaluated Rate Coefficients for Free Radical Polymerization. *Macromol. Chem. Phys.* **2004**, *205*, 2151–2160.
(22) Beuermann, S.; Buback, M. Rate Coefficients of Free-Radical Polymerization Deduced from Pulsed Laser Experiments. *Prog. Polym. Sci.* **2002**, *27*, 191–254.
(23) Plessis, C.; Arzamendi, G.; Leiza, J. R.; Schoonbrood, H. A. S.; Charmot, D.; Asua, J. M. Modeling of Seeded Semibatch Emulsion Polymerization of *n*-BA. *Ind. Eng. Chem. Res.* **2001**, *40*, 3883–3894.
(24) Former, C.; Castro, J.; Fellows, C. M.; Tanner, R. I.; Gilbert, R. G. Effect of Branching and Molecular Weight on the Viscoelastic Properties of Poly(butyl acrylate). *J. Polym. Sci., Part A: Polym. Chem.* **2002**, *40*, 3335–3349.
(25) Grady, M. C.; Simonsick, W. J.; Hutchinson, R. A. Studies of Higher Temperature Polymerization of *n*-Butyl Methacrylate and *n*-Butyl Acrylate. *Macromol. Symp.* **2002**, *182*, 149–168.
(26) Plessis, C.; Arzamendi, G.; Leiza, J. R.; Schoonbrood, H. A. S.; Charmot, D.; Asua, J. M. A Decrease in Effective Acrylate Propagation Rate Constants Caused by Intramolecular Chain Transfer. *Macromolecules* **2000**, *33*, 4–7.
(27) Nikitin, A. N.; Castignolles, P.; Charleux, B.; Vairon, J. P. Determination of Propagation Rate Coefficient of Acrylates by Pulsed-Laser Polymerization in the Presence of Intramolecular Chain Transfer to Polymer. *Macromol. Rapid Commun.* **2003**, *24*, 778–782.
(28) Plessis, C.; Arzamendi, G.; Alberdi, J. M.; van Herk, A. M.; Leiza, J. R.; Asua, J. M. Evidence of Branching in Poly(butyl acrylate) Produced in Pulsed-Laser Polymerization Experiments. *Macromol. Rapid Commun.* **2003**, *24*, 173–177.
(29) Tanaka, K.; Yamada, B.; Fellows, C. M.; Gilbert, R. G.; Davis, T. P.; Yee, L. H.; Smith, G. B.; Rees, M. T. L.; Russell, G. T. Pulsed-Laser Polymerization-Gel Permeation Chromatographic Determination of the Propagation-Rate Coefficient for the Methyl Acrylate Dimer: A Sterically Hindered Monomer. *J. Polym. Sci., Part A: Polym. Chem.* **2001**, *39*, 3902–3915.
(30) Maeder, S.; Gilbert, R. G. Measurement of Transfer Constant for Butyl Acrylate Free-Radical Polymerization. *Macromolecules* **1998**, *31*, 4410–4418.
(31) Pierik, S. C. J.; van Herk, A. M.; Plessis, C.; van Steenis, J. H.; Loonen, T.; Bombeeck, A. A Pulsed Light Reactor for Molecular Weight Control in Free-radical Polymerization. *Eur. Polym. J.* **2005**, *41*, 1212–1218.

MA071625L